The Astrophysical Journal, 789:162 (13pp), 2014 July 10 doi:10.1088/0004-637X/789/2/162

DYNAMIC PROPERTIES ALONG THE NEUTRAL LINE OF A DELTA SPOT INFERRED FROM HIGH-RESOLUTION OBSERVATIONS

A. Cristaldi[1,7,8], S. L. Guglielmino[1], F. Zuccarello[1], P. Romano[2], M. Falco[1], L. Rouppe van der Voort[3], J. de la Cruz Rodríguez[4], I. Ermolli[5], and S. Criscuoli[6]

[1] Dipartimento di Fisica e Astronomia-Sezione Astrofisica, Università di Catania, via S. Sofia 78, I-95123 Catania, Italy
[2] INAF-Osservatorio Astrofisico di Catania, via S. Sofia 78, I-95123 Catania, Italy
[3] Institute of Theoretical Astrophysics, University of Oslo, P.O. Box 1029 Blindern, N-0315 Oslo, Norway
[4] Institute for Solar Physics, Department of Astronomy, Stockholm University, Albanova University Center, SE-10691 Stockholm, Sweden
[5] INAF-Osservatorio Astronomico di Roma, via Frascati 33, I-00040 Monte Porzio Catone, Italy
[6] NSO-National Solar Observatory, Sacramento Peak Box 62, Sunspot, NM 88349, USA
Received 2013 October 30; accepted 2014 May 27; published 2014 June 25

ABSTRACT

Delta (δ) spots are complex magnetic configurations of sunspots characterized by umbrae of opposite polarity sharing a common penumbra. In order to investigate the fine structure of the region separating the two magnetic polarities of a δ spot, we studied the morphology, the magnetic configuration, and the velocity field in such a region using observations of active region (AR) NOAA 11267 obtained with the CRisp Imaging SpectroPolarimeter (CRISP) at the Swedish Solar Telescope on 2011 August 6. The analysis of CRISP data shows upflows and downflows of $\sim\pm3$ km s^{-1} in proximity of the δ spot polarity inversion line (PIL), and horizontal motions along the PIL of the order of ~1 km s^{-1}. The results obtained from the SIR inversion of CRISP data also indicate that the transverse magnetic field in the brighter region separating the two opposite magnetic polarities of the δ spot is tilted about $\sim45^{\circ}$ with respect to the PIL. *Solar Dynamics Observatory*/Helioseismic and Magnetic Imager observations confirm the presence of motions of $\sim\pm3$ km s^{-1} in proximity of the PIL, which were observed to last 15 hr. From the data analyzed, we conclude that the steady, persistent, and subsonic motions observed along the δ spot PIL can be interpreted as being due to Evershed flows occurring in the penumbral filaments that show a curved, wrapped configuration. The fluting of the penumbral filaments and their bending, continuously increased by the approaching motion of the negative umbra toward the positive one, give rise to the complex line-of-sight velocity maps that we observed.

Key words: Sun: activity – Sun: magnetic fields – Sun: photosphere – sunspots – techniques: high angular resolution

Online-only material: animation, color figures

1. INTRODUCTION

Active regions (ARs) containing δ configuration sunspots, i.e., spots of opposite polarity sharing the same penumbra, can evolve very rapidly, often giving rise to eruptive events, such as solar flares and coronal mass ejections, which may also be geo-effective. According to Zirin & Liggett (1987), δ spots can form in three main ways:

1. a single structure emerges with reverse polarity with respect to the Hale–Nicholson rules;
2. satellite dipoles emerge close to existing spots and the Emerging Flux Region expands, converting a preceding (in the sense of solar rotation) spot into a following spot or vice versa; or
3. a collision between two dipoles may occur so that opposite polarities are pushed together (Kunzel et al. 1961; Tang 1983).

Most violent flares seem to occur in the first two classes of δ spots, likely due to non-potential magnetic field topology and to a sheared polarity inversion line (PIL) that is the site of energy release. Therefore, identification of peculiar properties of plasma and magnetic fields in the region between the opposite magnetic polarities of δ spots may help clarify the dynamics and magnetic properties of these features, providing new insights useful to the understanding of the physical processes leading to eruptive phenomena.

Earlier observations show that the interface regions are characterized by strong downflows and highly sheared magnetic fields (Martínez Pillet et al. 1994), persistent convergent motions and abrupt changes in the magnetic field orientation (Lites et al. 2002), and strong shear flows and curved penumbral filaments (Denker et al. 2007). More recent observations also indicate submergence of a magnetic Ω-loop (Takizawa et al. 2012) and bending of penumbral filaments in the proximity of the PIL (Prasad Choudhary & Deng 2012). However, while the main characteristics of the penumbral magnetic field in sunspots are relatively well understood, it is not yet clear how the magnetic field lines and the embedded plasma flow change during the formation of a δ spot, and how they are pushed against each other in the region separating the two magnetic polarities.

In this paper, we present results obtained from the analysis of a δ spot observed with the very high spatial, temporal, and spectral resolution attainable at the Swedish 1 m Solar Telescope (SST) (0.″15). These observations, complemented with data acquired by the Helioseismic and Magnetic Imager (HMI) on board the *Solar Dynamics Observatory* (*SDO*) satellite, allowed us to study the morphological, magnetic, and dynamic properties of the region between the opposite polarities of a δ spot.

The paper is organized as follows. In Section 2, we describe the observations and the methods used to reduce the data. In Section 3, the data analysis is described, first using the

[7] Current Address: Dipartimento di Fisica, Università di Roma Tor Vergata, via della Ricerca Scientifica 1, I-00133 Rome, Italy.
[8] Current Address: INAF-Osservatorio Astronomico di Roma, via Frascati 33, I-00040 Monte Porzio Catone, Italy.

SDO/HMI data and then the high-resolution SST data. In Section 4, we discuss our results in the framework of previous observations, and in Section 5, we draw our conclusions.

2. OBSERVATIONS

The AR analyzed in this paper is NOAA AR 11267. It was observed on 2011 August 6, with the CRisp Imaging SpectroPolarimeter (CRISP; Scharmer et al. 2008) at the SST (Scharmer et al. 2003a) from 09:00:05 UT until 09:37:37 UT, at solar coordinates S17E24 (−350″, −360″), with heliocentric cosine angle $\mu = 0.84$.

The CRISP observations consist of full Stokes profile measurements of the Fe I line at 630.25 nm, and spectroscopic measurements along the profile of the Fe I line at 557.6 nm. Filtergrams in the core of the Ca II H line at 396.8 nm and in the wide band were acquired simultaneously with the Fe I data. The pixel size of the Fe I data is 0.″059 pixel^{-1} at 557.6 nm, while that of Ca II H filtergrams is 0.″034 pixel^{-1}. The field of view (FoV) of the CRISP data is 57.″5 × 57.″3.

CRISP acquired data every 4.4 pm along the Fe I line at 630.2 nm at 15 line positions from −30.7 pm to +30.7 pm with respect to the line center. We acquired 10 frames for each spectral point and for each polarization state of liquid crystals defining Stokes parameters. The temporal cadence of each complete spectropolarimetric scan along the Fe I line profile at 630.25 nm is ∼28 s. CRISP stopped acquiring data along this line profile at 09:30:16 UT. Moreover, CRISP acquired spectral data along the Fe I line profile at 557.6 nm, with a step of 3 pm covering a spectral range of 20 spectral points, from −27 pm to +27 pm with respect to the line center, and taking also a frame in the continuum at +66 pm. We acquired 20 frames for each spectral point. The temporal cadence of each complete scan of the Fe I line at 557.6 nm is ∼28 s. As concerns the blue channel (Ca II H line core and wide band), the temporal cadence of these data is 9 s.

The data were corrected using a standard reduction for dark current and flat field, and using the CRISPRED software (de la Cruz Rodríguez et al. 2014) to process the CRISP data. During the observations, the adaptive optics system of the SST (Scharmer et al. 2003b) was operating. To compensate for residual atmospheric aberrations, we applied the Multi-Object Multi-Frame Blind Deconvolution (MOMFBD; van Noort et al. 2005) technique, following a data reduction scheme described by Schnerr et al. (2011) but including a simplification in the flat-fielding process according to de la Cruz Rodríguez et al. (2013). Residual seeing distortions were compensated, after applying the MOMFBD technique, using a method described by Henriques (2012). Finally, the data set has been de-rotated, aligned, and de-stretched to compensate for rubber-sheet distortions as a function of time (Shine et al. 1994). Wide-band images, acquired simultaneously with the spectropolarimetric scans, were used as a so-called anchor channel to ensure precise alignment between the sequentially recorded CRISP narrow-band images and near diffraction-limited resolution has been achieved (0.″15 at 557.6 nm).

In order to study the dynamics in the observed FoV, we obtained the Doppler velocity of plasma motions by applying a Gaussian fit to the Fe I line profile at 557.6 nm with the MPFIT routine (Markwardt 2009) in IDL. The reference for the local frame of rest was calibrated by imposing that the plasma in a quiet Sun region has on average a convective blueshift for the Fe I 557.6 nm line (Dravins et al. 1981), corrected for the position on the solar disk according to Balthasar (1988). We obtain a value of $-0.368\,\mathrm{km\,s^{-1}}$, also in agreement with the theoretical estimation for $\mu = 0.8$ deduced by de la Cruz Rodríguez et al. (2011) using three-dimensional hydrodynamical simulations of LTE radiative transfer.

The CRISP observations were complemented with full-disk continuum filtergrams, longitudinal (line-of-sight, LOS) magnetograms, and Dopplergrams taken by the HMI (Scherrer et al. 2012) on board the *SDO* (Pesnell et al. 2012) in the Fe I line at 617.3 nm with a resolution of 1″. These data cover three days of observations, starting from 2011 August 5 at 00:10:25 UT until August 7 at 23:58:25 UT. They were analyzed to study the global characteristics and the temporal evolution of the AR. The cadence of these data, constructed using filtergrams from the HMI vector magnetic field series, is 12 minutes. LOS velocities were calibrated assuming that the velocity in sunspot umbrae is globally at rest. To this end, we defined sunspot umbrae as those pixels whose continuum intensity contrast I_c satisfies $I_c < 0.5$, where the contrast is defined as the ratio between the pixel continuum intensity and the average continuum intensity of a quiet Sun area in the FoV. All the *SDO*/HMI images were aligned, taking into account the solar differential rotation using the IDL *SolarSoft* package.

To co-align CRISP and *SDO*/HMI observations, we used the first spectral image in the sequence of CRISP data taken at 09:00:05 UT in the continuum of the Fe I 557.6 nm line and the *SDO*/HMI continuum image closest in time among the HMI Doppler camera data series with 45 s cadence, which was co-aligned with an *SDO*/HMI reference image in the LOS magnetograms series with 12 minute cadence. We used the IDL *SolarSoft* mapping routines to take into account the different pixel sizes. The displacement between the two images was obtained with cross-correlation techniques. From the *SDO*/HMI observations, we extracted sub-arrays, as shown in Figures 1 and 2. On the sub-arrays derived from the magnetograms, we computed the magnetic flux by taking into account projection effects due to the variation of the heliocentric cosine angle μ.

3. DATA ANALYSIS

3.1. NOAA 11267 evolution

We observed NOAA AR 11267 since it was still a recently formed AR consisting of two main sunspots of opposite polarity, with the preceding one characterized by a δ configuration. During its passage on the solar disk, this AR was classified as a $\beta\gamma\delta$ group and hosted five C-class flares. In particular, on 2011 August 6, i.e., the day of the CRISP observations, a C4.1 two-ribbon flare occurred at 08:37 UT in the δ spot, slightly before the SST observations.

Figure 1 (left panel) shows *SDO*/HMI continuum observations of the photospheric configuration of the AR at 09:10:25 UT on 2011 August 6 and the relevant *SDO*/HMI LOS magnetogram (right panel), which clearly shows that the western preceding sunspot has a δ configuration. The movie available in the online journal shows that the δ region emerges during the first hours of 2011 August 5, like a bipolar structure with reverse polarity with respect to the Hale rule (class I in Zirin & Liggett 1987), in between the diffuse, opposite polarities forming the AR.

Figure 2 shows the evolution of NOAA AR 11267 on 2011 August 6, from 00:10:25 UT until 21:10:25 UT, as depicted from a sequence of *SDO*/HMI continuum observations (left panels) and corresponding LOS magnetograms (right panels). From the comparison of the images in the top panels of Figure 2,

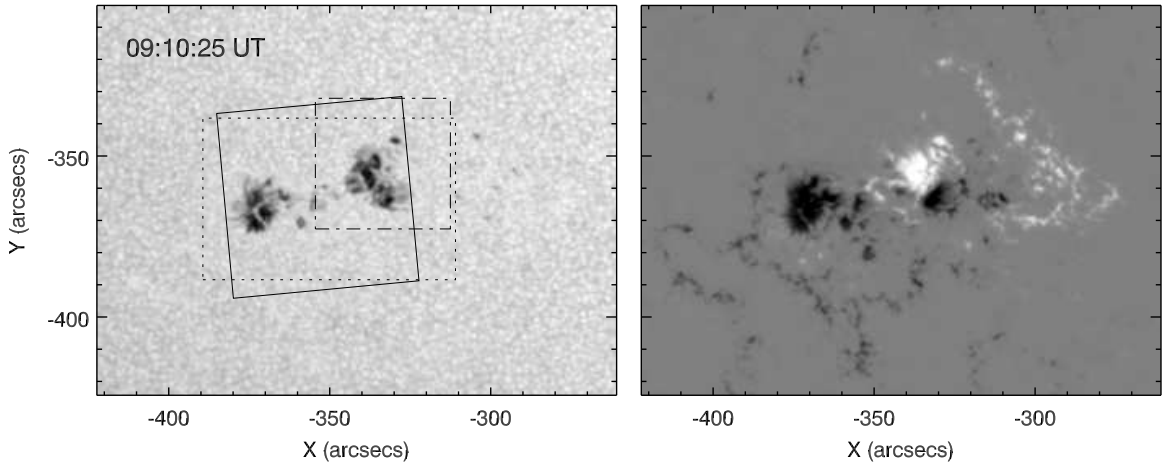

Figure 1. Left: *SDO*/HMI continuum image showing the photospheric configuration of NOAA AR 11267 at 09:10:25 UT on 2011 August 6. The preceding sunspot has a δ configuration. The solid line square indicates the FoV used for the SST acquisitions, the dotted line rectangle shows the *SDO*/HMI FoV used in Figure 2, and the dash–dotted line rectangle shows the *SDO*/HMI FoV used in Figures 4 and 5. Right: *SDO*/HMI magnetogram showing the magnetic configuration of the AR; the presence of both positive and negative polarities in the preceding sunspot is clearly observable. In this and in the following images, solar north is on the top, west is to the right.

(An animation of this figure is available in the online journal.)

we deduce that the preceding sunspot, characterized by positive polarity, is initially close to a wide region of negative polarity, but at this stage of the AR evolution, the negative polarity is not sufficiently intense to produce an umbra. In the second row of panels, relevant to 03:10:25 UT, the δ spot, indicated by an arrow in the magnetogram, forms due to the fact that the positive and negative polarities approach each other. The δ configuration takes place, arising from the coalescence of these structures of opposite polarity, with an increasing predominance of the positive polarity. The bottom panels of Figure 2 indicate that the structure persists during the selected time interval (the δ spot lifetime is ∼three days, while the AR disappears in ∼five days).

Figure 2 also shows that both main sunspots develop LBs during their evolution and that a bundle of small pores is located between the two main sunspots. During the analyzed time interval, the areas of the two umbral regions decrease, while the distance between the main sunspots increases.

Figure 3 displays the evolution of the magnetic flux in the whole AR during the three days of the analyzed *SDO*/HMI observations, from 00:10:25 UT on 2011 August 5, until 23:58:25 UT on August 7. The plot reports separately the negative flux in the sub-field comprised between [−341.″5, −261″] in the *X* direction in Figure 1 encompassing the δ spot (half-right part of the FoV), and that in the sub-field comprised between [−422″, −341.″5], containing the following sunspot and the diffuse negative polarity flux elements (half-left part of the FoV). With this choice we can distinguish the contribution of a possible emergence or variation of the negative flux in the δ spot area from that in the following polarity. We initially find a predominance of the negative magnetic flux (blue symbols) in the half-right part of the FoV, increasing during the first day (the maximum value measured is $\sim 1.3 \times 10^{21}$ Mx), followed by the first decrease phase. Then, there is a new flux increase, and finally a decreasing trend. The positive flux (red symbols) in the half-right part of the FoV increases almost continuously during the first day (maximum value $\sim 1.5 \times 10^{21}$ Mx) and later remains approximately constant. The negative magnetic flux (green symbols) in the half-left part of the FoV shows a clear increase during the first day, with a peak at about 2×10^{21} Mx, and it is followed by a slow decrease phase until the end of the observations. The green vertical band in Figure 3 indicates the time interval of CRISP observations, which is characterized by a decrease of the negative flux and almost constant positive flux in the analyzed AR.

Figure 4 shows a sequence of Dopplergrams of the δ spot that were derived from *SDO*/HMI data obtained on 2011 August 6, from 00:10:25 UT until 21:10:25 UT, with a cadence of 3 hr. Blue (red) indicates upward (downward) motions. We find both upflows and downflows (up to ∼3 km s^{-1}) in the region of interface between the opposite polarities of the δ spot, which persist for ∼15 hr at least. The relation of these LOS motions with the magnetic configuration in the region is clearly visible in Figure 5: the *SDO*/HMI magnetogram relevant to 09:10:25 UT is shown, with the same FoV of the Dopplergram displayed in Figure 4, and the LOS motions are overplotted as red (downward) and blue (upward) contours. Figure 5 distinctly shows the proximity of the upflows and downflows along the PIL separating the two magnetic polarities of the δ spot.

3.2. Analysis of CRISP Data

Figure 6 (left panel) shows the photospheric configuration of the AR as derived from the CRISP data in the continuum of the Fe I line at 557.6 nm. We find the presence of a LB in the eastern, negative sunspot (indicated by a red arrow). This LB has a typical structure consisting of a central dark lane and chains of small-scale bright granules at its sides (i.e., the so-called segmented LB; see, e.g., Thomas & Weiss 2004; Berger & Berdyugina 2003). The penumbral filaments seem to be present only at the umbra border not facing the other main sunspot, a characteristic that has been observed in some recent high-resolution observations relevant to the phase of formation of the penumbra (see, e.g., Schlichenmaier et al. 2010; Romano et al. 2013).

The preceding sunspot also shows segmented LBs separating some areas with the same positive magnetic polarity (compare Figure 6, left panel, with Figure 6, right column, bottom row). Conversely, the region between the opposite polarities of the δ spot, is similar to a bunch of sheared dark filaments interspersed with bright zones, lying almost tangentially to both opposite polarity umbra cores.

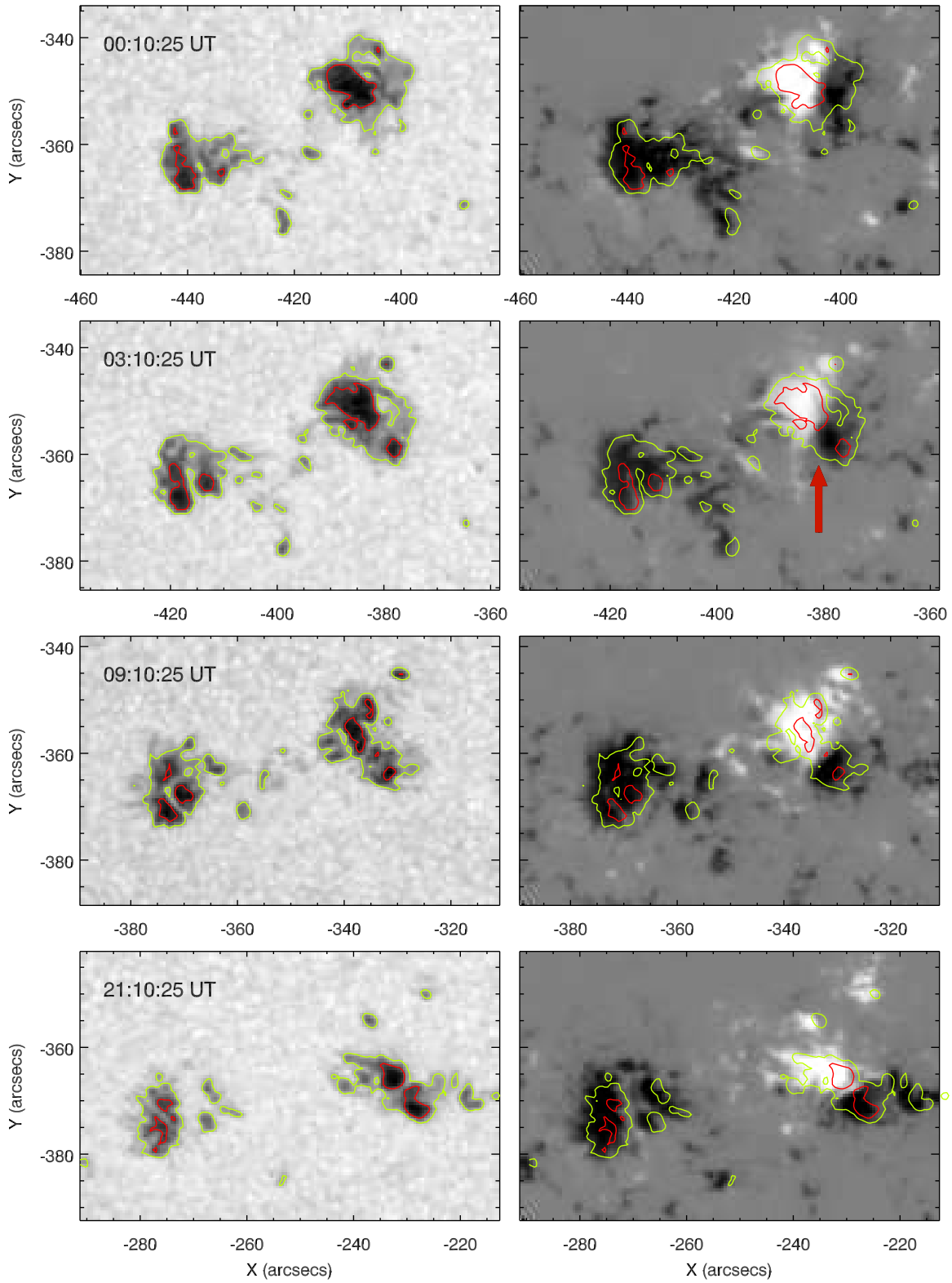

Figure 2. Sequence of *SDO*/HMI continuum images (left panels) and corresponding magnetograms (right panels) with the contours of umbrae ($I_c = 0.55$, red) and penumbrae ($I_c = 0.85$, yellow) overplotted in the studied AR at different observational times on 2011 August 6. White (black) areas on the magnetograms indicate positive (negative) polarities. The arrow in the magnetogram acquired at 03:10:25 UT indicates the δ spot. The FoV corresponds to the dotted rectangle indicated in Figure 1 (left panel).

(A color version of this figure is available in the online journal.)

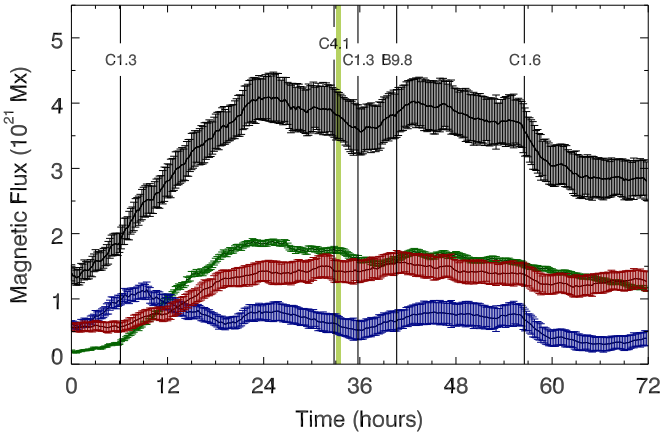

Figure 3. Evolution of magnetic flux in NOAA AR 11267 determined by *SDO*/HMI longitudinal magnetograms acquired from 00:10:25 UT on 2011 August 5 to 23:58:25 UT on August 7. Red (blue) symbols indicate the positive (negative) magnetic flux of the half-right of the FoV shown in Figure 1 (right panel) including the western leading δ spot, while green symbols indicate the negative magnetic flux of the remaining half-left part of the FoV (see the text for a more precise definition of the regions indicated with "half-right" and "half-left"). Black symbols refer to the total unsigned magnetic flux of the whole FoV. The bars indicate the standard deviation. The green vertical band delimits the time interval during which the observations at the SST were carried out. The vertical lines refer to the flares that occurred in the AR, labeled with their magnitude.

(A color version of this figure is available in the online journal.)

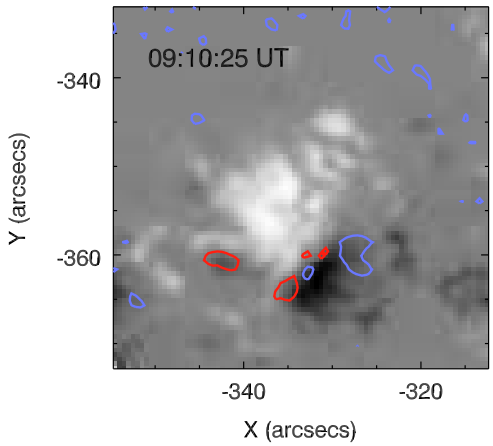

Figure 5. *SDO*/HMI magnetogram, acquired on 2011 August 6, with the contours of the downward and upward motions in the δ spot overplotted. Contour velocity values are -1 km s^{-1} (upflows, blue color) and 1 km s^{-1} (downflows, red color). The FoV is the same as in Figure 4.

(A color version of this figure is available in the online journal.)

The area of the eastern, positive umbra of the δ spot is $\sim$14 Mm^2, while the western (negative polarity) umbra has an area of $\sim$3 Mm^2. Figure 6 (left panel) also shows the sub-FoV (solid line) considered in the CRISP data to derive the results presented in the following.

Figure 6 (right column, upper row) shows the chromospheric configuration of the AR, as deduced from Ca II H observations (negative image). We notice bright regions in correspondence of the LB seen in the photospheric image (compare with Figure 6, left panel, green arrow), in agreement with previous observations that reported chromospheric activity above these structures (e.g., Berger & Berdyugina 2003; Bharti et al. 2007; Shimizu et al. 2009). Moreover, some brightenings are present near the western edge of the FoV just to the north of the negative polarity. We cannot exclude that these Ca II H brightenings, which extend well beyond the LBs, are also linked to the C4.1 flare that occurred in the AR slightly before the observations of the SST. On the other hand, we find that there is no such similar bright filamentary region in the area corresponding to the PIL separating the two polarities of the δ spot (compare Figure 6, left panel, with Figure 6, right column, upper row).

Figure 7 (top panel) displays plasma motions in the sub-FoV of the CRISP data. Downward and upward motions along the PIL between the opposite polarities of the δ spot are indeed present. In Figure 6 (right column, upper row) the contours of these velocities are overplotted on the chromospheric Ca II H image. The resulting map clearly shows that the strongest

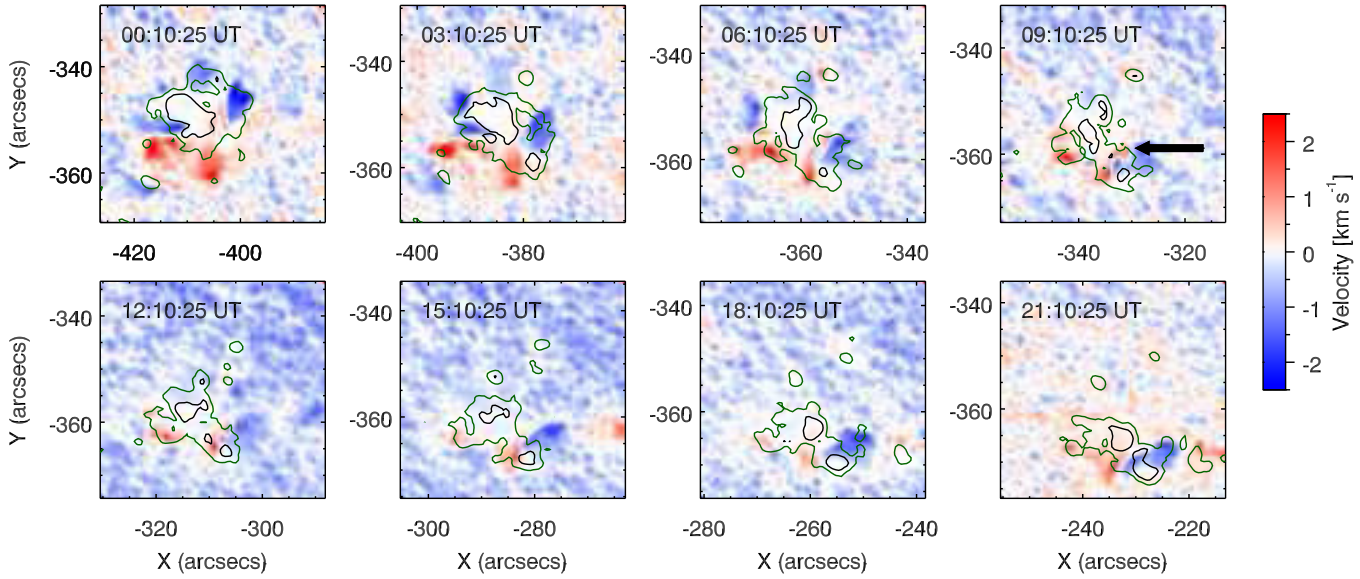

Figure 4. Sequence of *SDO*/HMI Dopplergrams acquired on 2011 August 6 with the contours of the umbrae ($I_c = 0.55$, black) and penumbrae ($I_c = 0.85$, green) overplotted in the δ spot. Blue (red) indicates upflows (downflows). The arrow in the Dopplergram relevant to 09:10:25 UT indicates the approximate location of the PIL separating the two opposite polarities of the δ spot. The FoV corresponds to the dash–dotted rectangle indicated in Figure 1 (left panel).

(A color version of this figure is available in the online journal.)

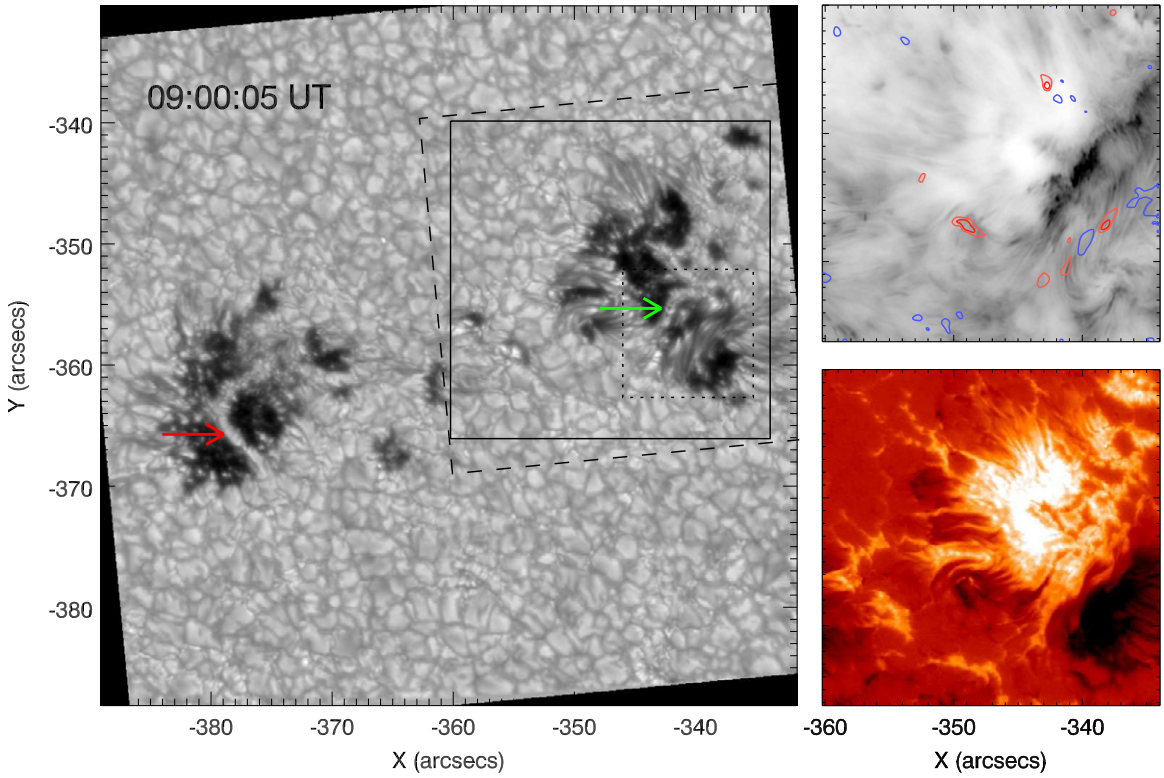

Figure 6. Left: NOAA AR 11267 observed by the SST in the continuum of the Fe I line at 557.6 nm. The image is correctly rotated, taking into account the *SDO* images. The SST FoV is 57.″5 × 57.″3. The *x*- and *y*-axes are given in disk center coordinates. The dashed line square indicates the part of the SST FoV selected for the SIR inversion, the solid line square indicates the FoV used to show the results in the following figures, and the dotted line box indicates the FoV of the zoomed region displayed in Figure 11. The red and green arrows indicate the LBs observed in the following and leading sunspots, respectively. Right: upper row: Ca II H image (color inverted–negative image of the Ca II H intensity) of NOAA AR 11267 with contours of velocities in the range −3, −1.5 km s^{-1} (blue) to +1.5, +3 km s^{-1} (red). Bottom row: map of the longitudinal polarization signal obtained with the integrated Stokes *V* parameter. The FoV is that indicated with the solid line square in the left panel. (A color version of this figure is available in the online journal.)

upward and downward motions correspond to regions far from the bright features that are situated above the segmented LB observed in the continuum image.

We notice that along the δ spot PIL (indicated by a black solid line in Figure 7, top panel), there are strong LOS motions, both downward and upward. We have selected two regions (named *A* and *B*, characterized respectively by downward and upward motions) in the area separating the two magnetic polarities of the δ spot, to further investigate the velocity fields in this interface region. We have studied the temporal behavior of the LOS motions in these areas, with dimension of 9 × 9 pixels, corresponding to 0.″53 × 0.″53 (see Figure 7, top panel). The results of the evolution of these motions are shown in Figure 7 (bottom panel). The velocities (both positive and negative) are quite variable during the analyzed time interval, not showing a clear systematic trend during the whole observation (i.e., for about 37 minutes), but still they remain on average within 2 and 3 km s^{-1}. This result indicates that these motions are not related to the C4.1 flare that occurred slightly before the beginning of the SST observations.

Finally, we have investigated whether horizontal motions are present in the analyzed region, with particular interest in the region between the two magnetic polarities of the δ spot. Figure 8 shows the horizontal velocity field derived from application of the Local Correlation Tracking (LCT; November & Simon 1988) to Ca II H wide-band images. We used a FWHM of the apodization window of 0.″85 and a time interval of 54 s between the two successive frames to be compared, averaged over 30 minutes. The result is shown in Figure 8. We find that a pattern of horizontal motion is present across the δ spot PIL (see the white circle in Figure 8), with an average velocity of the order of 1 km s^{-1}, mostly oriented toward the umbra of positive polarity, nearly perpendicular to the PIL itself and to the tangential penumbral filaments. Note that proper motions of individual granules and penumbral filaments can still be present in such a flow map based on a 30 minute average (Verma & Denker 2011).

3.3. CRISP Data Inversion

The Stokes profiles of the first scan of CRISP measurements of the Fe I 630.25 nm line, characterized by excellent seeing conditions, acquired at 09:00:05 UT, was inverted using the SIR code (Ruiz Cobo & del Toro Iniesta 1992). A single-component inversion was applied to the sub-array of 500 × 500 pixels, indicated with a dashed line square in Figure 6 (left panel).

The temperature stratification of each component was modified with three nodes, using the stratification of the Harvard–Smithsonian Reference Atmosphere (HSRA; Gingerich et al. 1971) as an initial guess. The other physical parameters (LOS velocity, field strength, inclination, and azimuth angles) were assumed to be constant with height. The stray-light contamination was modeled by averaging over all Stokes *I* spectra in the 64 pixels characterized by the lowest polarization degree over the sub-array of 500 × 500 pixels, indicated with a dashed line square in Figure 6 (left panel). The finite spectral resolution of the instrument was taken into account during the inversion process using the spectral point-spread function of

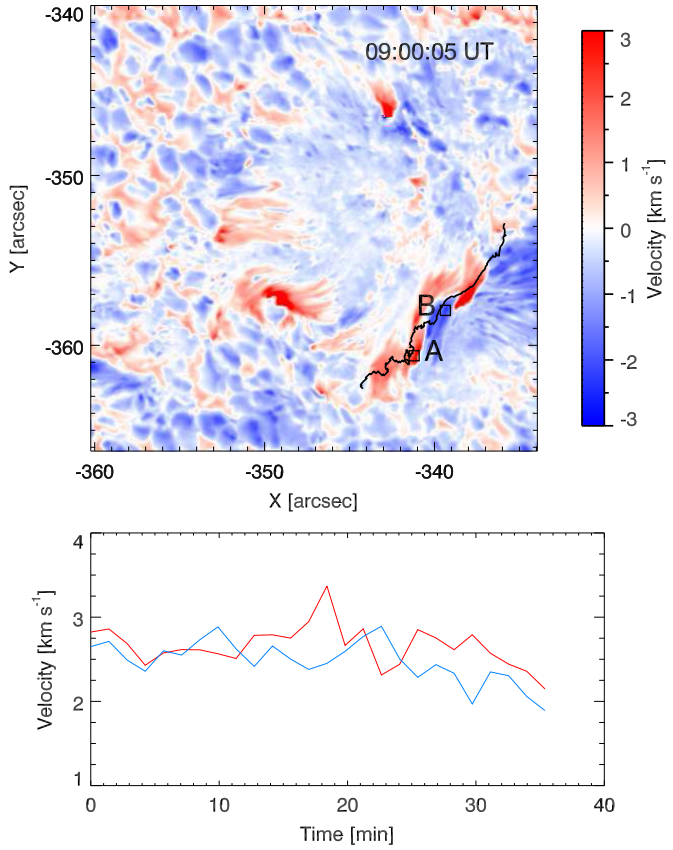

Figure 7. Top panel: Doppler map of the AR obtained from the shifts in the Fe I line at 557.6 nm; the black contours indicate the location of the PIL separating the two magnetic polarities of the δ spot. The FoV refers to the solid line square in Figure 6 (left panel). The squares labeled *A* and *B* in proximity of the PIL frame the regions of downflow and upflow, respectively, and were selected to determine the velocity evolution, reported in the bottom plot. Bottom panel: plot of the Doppler velocity (absolute values). The red (blue) curve refers to square *A* (*B*).

(A color version of this figure is available in the online journal.)

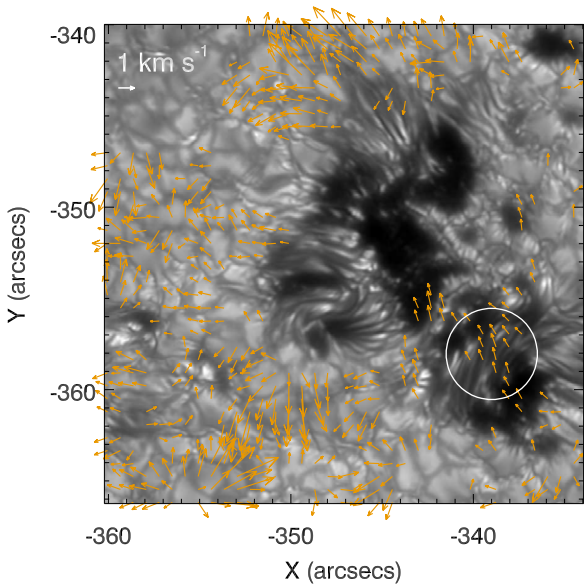

Figure 8. Ca II H wide-band image with the horizontal velocity field inferred using the LCT technique overplotted. The white arrow at the top-left corner of the image represents a horizontal velocity of 1 km s^{-1}. The white circle highlights the horizontal motions in proximity to the δ spot PIL. Points with horizontal velocities lower than 0.5 km s^{-1} are not indicated.

(A color version of this figure is available in the online journal.)

CRISP. The results were successively transformed into the local solar frame, because the position of the AR was not close to the solar disk center ($\mu = 0.84$).

We solved the 180° ambiguity of the azimuth angle using the AMBIG code, which implements a minimum energy method, as described by Leka et al. (2009). The LOS velocities derived from the SIR data inversion were calibrated assuming that plasma in sunspot umbrae (with continuum intensity $I_c < 0.5$) is globally at rest.

The results obtained are shown in Figure 9, where the maps of the magnetic field strength, transverse and longitudinal field components, and LOS velocities are displayed. From an inspection of the map of the magnetic field strength (Figure 9, top left panel), we deduce that the intensity of the magnetic field in the region between the opposite polarities of the δ spot is on average 1600 G, i.e., not as low as it appears in the region corresponding to the segmented LB (∼900 G). The map of the transverse magnetic field (Figure 9, top right panel) shows that there is a wide region at the interface between the two magnetic polarities of the δ spot, where the magnetic field is almost parallel with respect to the solar photosphere. Figure 9 (bottom left panel) shows the longitudinal magnetic field map with superimposed arrows whose length is proportional to the transverse component of the magnetic field, and whose direction indicates the azimuth direction. This map indicates that the magnetic field lines between the two opposite polarities of the δ spot are tilted with respect to the direction along which the two umbrae face each other. Note that the dark fibril-like structures observed in photospheric continua around this interface region appear to follow the horizontal field lines.

Furthermore, the map of the LOS velocity field (Figure 9, bottom right panel) indicates that along the δ spot PIL downflows (red) and upflows (blue) are present. The velocity measured in both upward and downward motions reach absolute values of ∼3 km s^{-1}, therefore confirming the results obtained from the analysis of *SDO* Dopplergrams and SST measurements along the Fe I line at 557.6 nm.

In order to highlight the dynamical and magnetic differences between the δ spot PIL and the LB present in the leading sunspot, indicated with a green arrow in Figure 6 (left panel), both areas being characterized by evident magnetic field discontinuities, we select two linear paths crossing each of these regions. Figure 10 (left panel) displays an image of the δ spot in the continuum of the Fe I line at 630.25 nm; the green and blue segments show two selected paths along the LB where the variation of continuum intensity, LOS velocity, magnetic field strength, and magnetic field inclination as a function of position have been measured. The red and violet segments indicate the path along the δ spot PIL where we have calculated the same parameters. Each segment has a length of ∼1 Mm. In Figure 10 (right panel), we plot the results of these measurements. From the top left panel, clockwise: continuum intensity normalized to the quiet Sun, LOS velocity, magnetic field strength, and magnetic field inclination as a function of pixel position along the LB (green and blue lines) and along the PIL (red and violet lines), with colors referring to the segments drawn in the same Figure 10 (left panel). In each plot, the pixel position 0 corresponds to the most northeastern location for each segment.

We find that along the segments crossing the LB, the continuum intensity reaches values up to 1.15 I_c, while in the region separating the two opposite polarities along the δ spot PIL, the

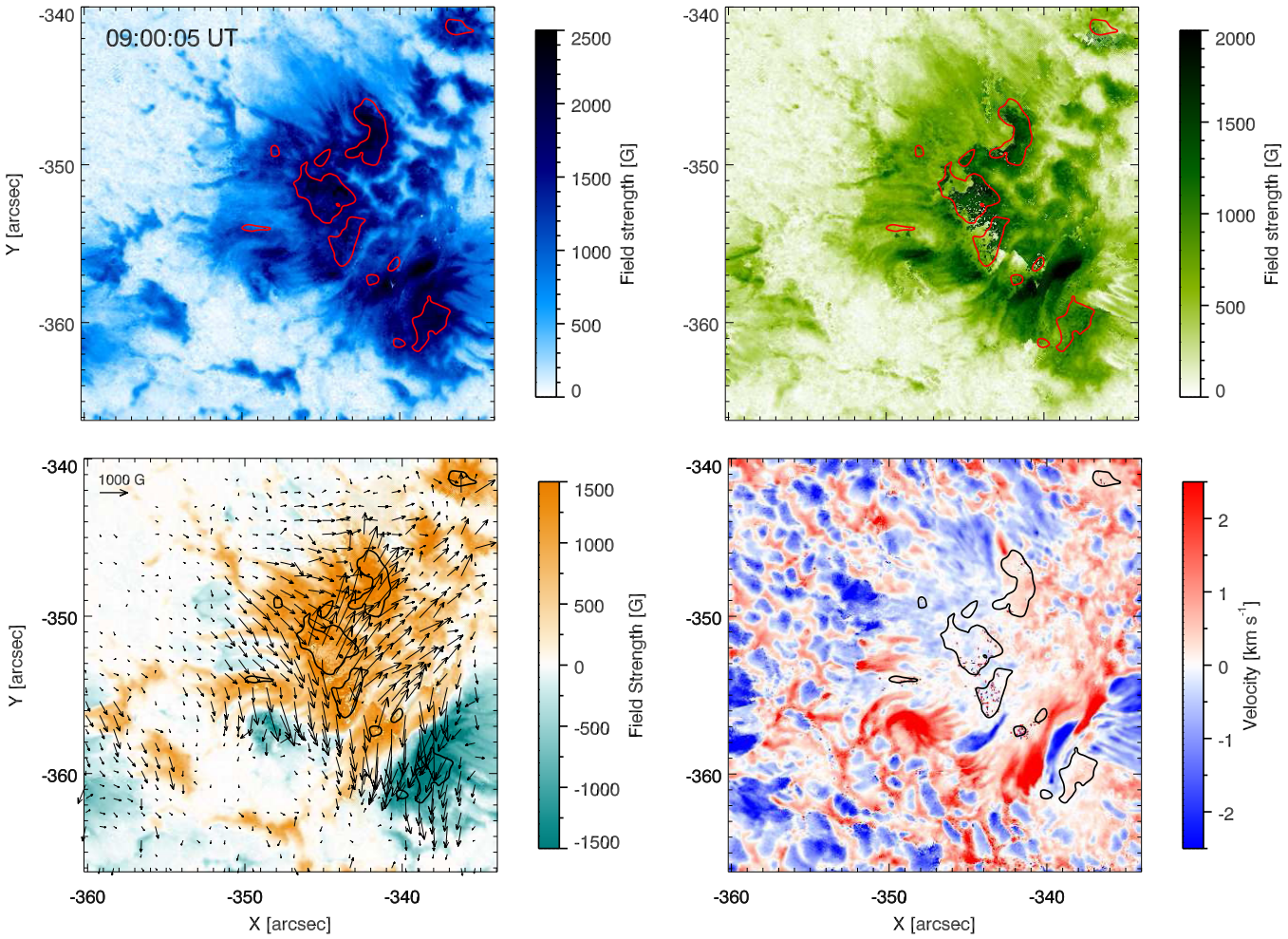

Figure 9. Results obtained from the SIR inversion of the SST data. Top left panel: magnetic field strength. Top right panel: transverse magnetic field in the local solar frame. Bottom left panel: longitudinal magnetic field in the local solar frame; the arrow length is proportional to the transverse component of the magnetic field, while their directions indicate the azimuth direction. The arrow at the top left corner of this map represents a horizontal field of 1000 G. Points with a horizontal field lower than 200 G are not indicated. Bottom right panel: LOS velocity field. The contours indicate the isophotes of the δ spot umbrae at $I_c = 0.5$.

(A color version of this figure is available in the online journal.)

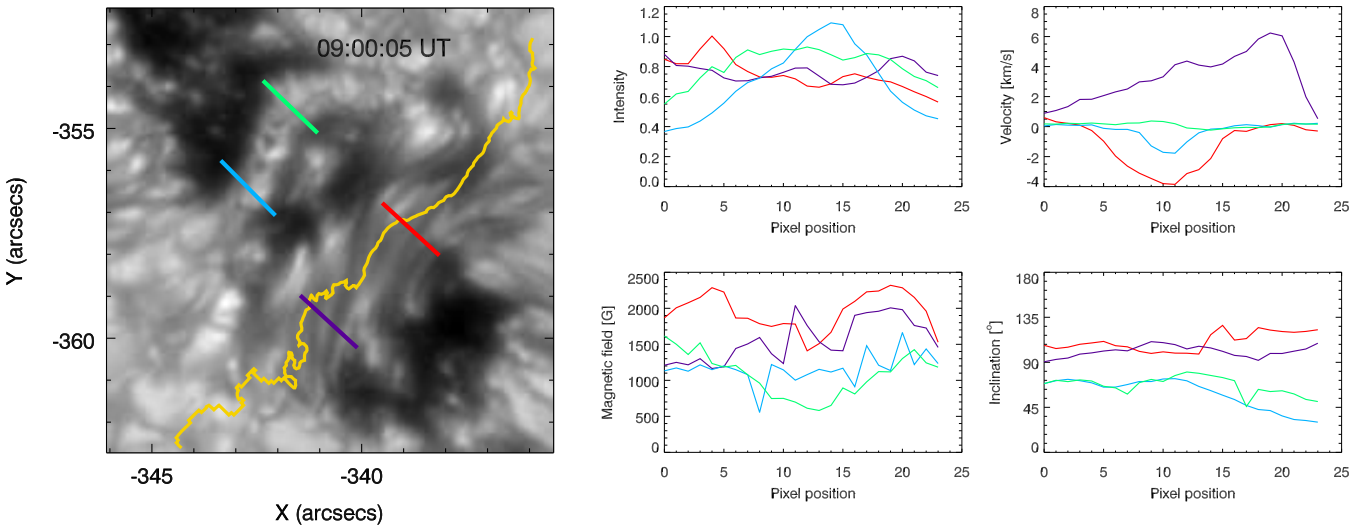

Figure 10. Left: image of the δ spot in the continuum of the Fe I line at 630.25 nm; the FoV is indicated in Figure 6 (left panel), with the dotted line square. The green and blue segments show the paths along the LB where the variation of brightness intensity, LOS velocity, magnetic field intensity, and magnetic field inclination as a function of position has been determined. The red and violet segments indicate the path along the δ spot PIL where the same parameters have been measured. The yellow contours indicate the PIL. Right: from top left, in the clockwise direction: continuum intensity normalized to the quiet Sun, LOS velocity, magnetic field inclination, and magnetic field intensity as a function of position along the LB (green and blue lines) and the δ spot PIL (red and violet lines). The pixel position 0 corresponds to the most northeastern location for each segment.

(A color version of this figure is available in the online journal.)

values can reach a maximum of $1.0\,I_c$. We remark that these values are on average lower than in the LB. Besides, the velocity pattern in the segments crossing the LB is different for the green (almost constant) and for the blue segment, as in the latter the presence of a central region of upflow is observable. In the red segment analyzed across the PIL, we note that in the central part the LOS velocity shows an upward motion, higher than in the blue segment crossing the LB; on the other hand, the pattern measured in the violet segment shows that the LOS velocity (positive, indicating a downflow) increases as the negative umbra is approached. We also find that the magnetic field strength is higher in both segments along the PIL in comparison to the values detected across the LB. Finally, the magnetic field inclination in both the segments crossing the PIL indicates that here the field is almost horizontal, while the inclination in the LB segments is $\sim 45^\circ$ or lower.

4. COMPARISON WITH PREVIOUS RESULTS

The analysis of *SDO*/HMI observations indicates the presence of a δ configuration in the preceding sunspot of NOAA AR 11267. The region between the opposite polarities of the δ spot is characterized by the presence of steady, persistent ($\sim$15 hr) patches of downward and upward motions up to $\sim 3\,\mathrm{km\,s^{-1}}$ on 2011 August 6.

High spatial resolution ($\sim 0\farcs15$) observations acquired with CRISP at the SST on the same day during a time interval of $\sim$37 minutes confirm the presence of these motions (see Figure 7). Besides, the CRISP data in the continuum of the Fe I line at 557.6 nm show that this region, which is characterized by an intensity contrast I_c between 0.6 and 1.0 with respect to the undisturbed photosphere, consists of a bundle of dark, curved filaments that appear almost tangential to both the positive and the negative umbra cores.

On the other hand, we find an indication of shearing of the magnetic field lines along the PIL of the δ spot (see Figure 9, bottom right panel), where the orientation and the direction of the transverse magnetic field reflect the morphology of the dark filaments observed in this area in photospheric continuum images. These results confirm previous findings reported in the literature (see below, e.g., Denker et al. 2007). Along the δ spot PIL we observe that the magnetic field strength appears to be lower than in the umbral cores, but on average higher than in the LB crossing the positive polarity umbra core (see, e.g., Figure 10).

Martínez Pillet et al. (1994), from the analysis of HAO/NSO Advanced Stokes Polarimeter (ASP) data with a spatial resolution of $1''$ of NOAA AR 7201, found evidence of strong downflows close to the neutral line of a δ spot. The observed flows were as large as $14\,\mathrm{km\,s^{-1}}$, suggesting, at a photospheric level, the presence of a supersonic flow. In the same FoV, an upflow of $\sim 1.5\,\mathrm{km\,s^{-1}}$ was also detected. Both downward and upward motions were observed to persist for the entire observation time, i.e., for three hours. Horizontal motions were detected in the analyzed region, but not in the proximity of the δ spot. Moreover, the photospheric magnetic field was aligned along the neutral line and it was possible to establish that the strong downflows were coincident with a highly sheared magnetic field at the neutral line. Taking into account that during the time interval analyzed no visible change in the magnetic configuration was detected, Martínez Pillet et al. (1994) concluded that the observed downflow could not result from a process of magnetic reconnection, but that nonlinear phenomena in the chromosphere and transition region were responsible for the observed high speeds.

Lites et al. (2002) studied a δ spot using ASP observations of the NOAA AR 7205, carried out on 1992 June 24, when the AR was located at N10W60. The δ spot, larger and more complex than that of NOAA AR 7201 (Martínez Pillet et al. 1994), was present in the leading polarity of the AR, and the PIL between the two magnetic polarities of the δ spot was characterized by Doppler shifts in the range $\pm 3\,\mathrm{km\,s^{-1}}$. However, in some locations along the PIL, evidence of flow speeds comparable to the sound velocity was found. Abrupt changes in the magnetic field orientation were detected along the PIL, as well as significant Stokes V asymmetries, the latter probably being an indication either of unresolved multiple magnetic components with large relative motions along the LOS or large velocity gradients, or both. Using the available data set, the authors came to the conclusion that the δ spot had a convex magnetic field topology. The results of a Milne–Eddington inversion with two magnetic components gave an indication of a persistent convergence zone along the PIL, leading the authors to the conclusion that the convergent motions had their origin in the Evershed flow (Evershed 1909) and could be due to fluted penumbral filaments with opposing flows in interleaved magnetic field lines.

Denker et al. (2007) stressed that strong shear flows are often observed along the PIL of flaring δ spots (see also Denker & Wang 1998). Along these shear flows, strongly curved penumbral filaments, almost tangential to the sunspot umbra, rather than the typical radial filamentary structure of the single-polarity sunspot penumbra, were observed. The authors studied a δ spot in NOAA AR 10756, characterized by shearing motions along the PIL, not correlated with changes in the local magnetic shear. The AR was observed on 2005 May 2, at S08W23, when it was already in a decaying phase; during its passage on the solar disk the AR produced several C-class flares. In NOAA AR 10756, the leading sunspot had predominantly negative polarity, and a small δ configuration with positive polarity was detected in its southern part. In the umbra of the δ spot, several faint umbral dots were observed. The penumbral filaments on the opposite side of the main spot had a typical outward radial direction, while the penumbral filaments facing the main spot (extending for more than $25''$) were strongly curved and wrapped around the umbra of the δ spot. These almost tangential penumbral filaments provided an indication of highly twisted (sheared) magnetic field lines.

Denker et al. (2007) could also determine that the penumbral filaments had a counterclockwise twist, leading to strong shear flows at the interface of the two penumbrae. Moreover, the curved penumbral filaments at the interface of the two umbral cores were much wider than those extending radially outward in the other sides. The horizontal and the LOS velocity reached up to $1.8\,\mathrm{km\,s^{-1}}$ and $2.5\,\mathrm{km\,s^{-1}}$, respectively. The authors stated that the proximity of two penumbrae with colliding outflows could result either in the subduction of one flow pattern or to horizontal deflection of the opposing flows. The line separating upflows and downflows follows the PIL, probably indicating that the penumbrae of the main and the δ spot behave as separate entities, so that the Evershed flow is deflected. Typical horizontal velocities reached $1.25\,\mathrm{km\,s^{-1}}$, while the magnetic shear along the PIL increased from 9° to 21° in about 5 hr.

Compared with the findings of Martínez Pillet et al. (1994), reporting downflows up to $14\,\mathrm{km\,s^{-1}}$ along the δ spot PIL and

an upward flow of 1.5 km s^{-1} in a nearby region, in the analysis of Denker et al. (2007), the flow kernels appear as pairs of opposite flows (lasting from 30 minutes to 3 hr) on both sides of the strongest magnetic field gradient at the interface of the opposite polarity umbrae. The main conclusion of this work was that these persistent flows cannot be attributed to flaring activity, but the observed photospheric flows are related to the magnetic field lines harboring the more horizontal Evershed flow channels.

Takizawa et al. (2012), using *SOHO*/MDI dopplergrams and magnetograms, measured in NOAA AR 9957 (a $\beta\gamma\delta$ rapidly decaying AR) downflow motions of 1.5–1.7 km s^{-1} for ~12 hr along the PIL of a δ spot region. Moreover, using the LCT technique, the authors detected converging horizontal flows toward the PIL for ~5 hr in the same areas where the downflows (not accompanied by any upward motion or any flaring activity) were observed. From the analysis of Huairou Solar Observing Station vector magnetograms, it was found that the magnetic field was parallel to the solar surface along the PIL. In conclusion, taking into account that in the downflow region penumbral structures were observed to decay, the authors could establish that the phenomenon was caused by submergence of a magnetic Ω-loop.

Prasad Choudhary & Deng (2012) studied NOAA AR 9664 and observed six downflow regions in proximity of the PIL (three at each polarity), with Stokes *V* profiles normal in the chromosphere but anomalous in the photosphere, and Stokes *I* profiles symmetric in the chromosphere but highly asymmetric in the photosphere. The velocities measured at the downflow regions were supersonic and lasted for about six hr. These authors proposed that a possible origin of these features could be the bending of penumbral Evershed flow channels. More precisely, taking into account that a *normal* sunspot has Evershed flow channels where the plasma flows almost parallel to the solar surface, these channels can get bent downward when they encounter the strong vertical field of another sunspot. Therefore, when this interface region is located between two opposite polarities sharing the same penumbra, i.e., as in a δ spot, the presence of strong downflows indicates the abrupt bending of the penumbral filaments in proximity of the PIL.

More recently, Balthasar et al. (2014) presented the results obtained from near-infrared observations in the Fe I 1078.3 nm and Si I 1078.6 nm lines carried out with the Tenerife Infrared Polarimeter at the Vacuum Tower Telescope (von der Lühe 1998) and relevant to NOAA AR 11504, observed on 2012 June 17. Balthasar et al. (2014) studied the magnetic and velocity fields along the neutral line of a δ spot present in the AR and found a smooth transition of the vector magnetic field from the main umbra to the δ spot umbra and a discontinuity of the horizontal magnetic field at some distance from the δ spot umbra on the PIL. The analysis also showed the presence of chromospheric upflows and downflows up to 8 km s^{-1} near the PIL, as well as motions interpreted as Evershed flows from the main umbra, ending in correspondence with a line dividing the spot into two parts.

We also recall the analysis carried out on NOAA AR 10930, where a δ spot exhibiting considerable rotation (up to 8° hr^{-1}) of the δ umbra, was observed by Min & Chae (2009). In particular, this analysis shows that in the region between the opposite polarity umbrae, the penumbral filaments, initially directed outward, due to the δ spot rotation later become very curved, until those closer to the δ umbra are tangential to it. Another effect of the δ spot counterclockwise rotation is the formation of a sigmoid, which was observed in *TRACE* images. Concerning the effect of umbra rotation on the shape of the penumbral filaments between the umbrae of opposite polarity, we can immediately exclude that such a phenomenon took place in the leading spot of the AR analyzed in our study, as can be inferred, e.g., from Figures 2 and 8.

Moreover, in another study relevant to NOAA AR 10930, Deng et al. (2011) detected for the first time the enhancement of a sheared Evershed flow along the neutral line after an X6.5 flare and interpreted this effect in the framework of a change of connectivity of penumbral field lines, such that the originally fanning out field lines at the two sides of the neutral line got connected as a consequence of the magnetic field restructuring during the flare. In particular, the Evershed flow detected using the LCT technique increased from 330 m s^{-1} to 400 m s^{-1}. This increase was observed until about one hr after the X6.5 flare, i.e., until the end of the available data. Another characteristic outlined by Deng et al. (2011) is that the region between the two magnetic polarities is dominated by the penumbra of the negative umbra and that penumbrae of the positive umbra almost vanish at the interface; therefore, a sheared Evershed flow of predominantly one direction was observed. When comparing these results with the outcomes of our study, we can see that there are major differences, some of them due to the fact that the Evershed flows observed by Deng et al. (2011) are detected (due to the observational data set) for a much shorter time interval, and others due to the different distribution of the penumbrae between the two magnetic polarities. It is, however, interesting to note that when the penumbral filaments are tangential to the umbrae border, the Evershed flow can become very enhanced.

In our analysis, we find that the region hosting the PIL of the δ spot shows motions along the LOS of the order of 3 km s^{-1}. Based on their lifetime (longer than 15 hr, as deduced from *SDO*/HMI Dopplergrams), these motions cannot be totally ascribed to the C-class flares that occurred in the AR on August 6. Therefore, they should be due to other causes; in the following we will examine three possible reasons for their origin and persistency, the emergence of new magnetic flux, submergence of an Ω-loop, or presence of velocity fields related to the Evershed flow.

The spatial configuration of the LOS velocities illustrated in Figure 7 (top panel) for the Fe I 557.6 nm line and in Figure 9 (bottom right panel) for the Fe I 630.25 nm line allow us to discard the hypothesis that the observed plasma motions of the PIL are generated by the emergence of a bundle of magnetic field lines, as for instance of an arch filament system (AFS; Bruzek 1967; Spadaro et al. 2004; Zuccarello et al. 2005). In fact, there is no clear signature of the emergence of magnetic flux along the δ spot PIL in the data (compare with Figure 2 and with the red and blue symbols in Figure 3 between 24 and 36 hr). Besides, AFSs are generally oriented perpendicular to the PIL, so we should expect that such features, which should be co-spatial with the dark loops seen in Ca II H images, present the upward (blue) region above the PIL and the downflow regions at both sides (see, for instance, Figure 11 in Zuccarello et al. 2005), while this is not the velocity pattern we observe. Thus, we can exclude that the observed motions could have their origin in the emergence of a bundle of flux tubes between the opposite polarities of the δ spot.

We can examine the opposite situation, i.e., the submergence of an Ω-loop. Takizawa et al. (2012) described two scenarios for such a process: (1) either the moat flows act on the magnetic flux above the solar photosphere and drag the flux downward,

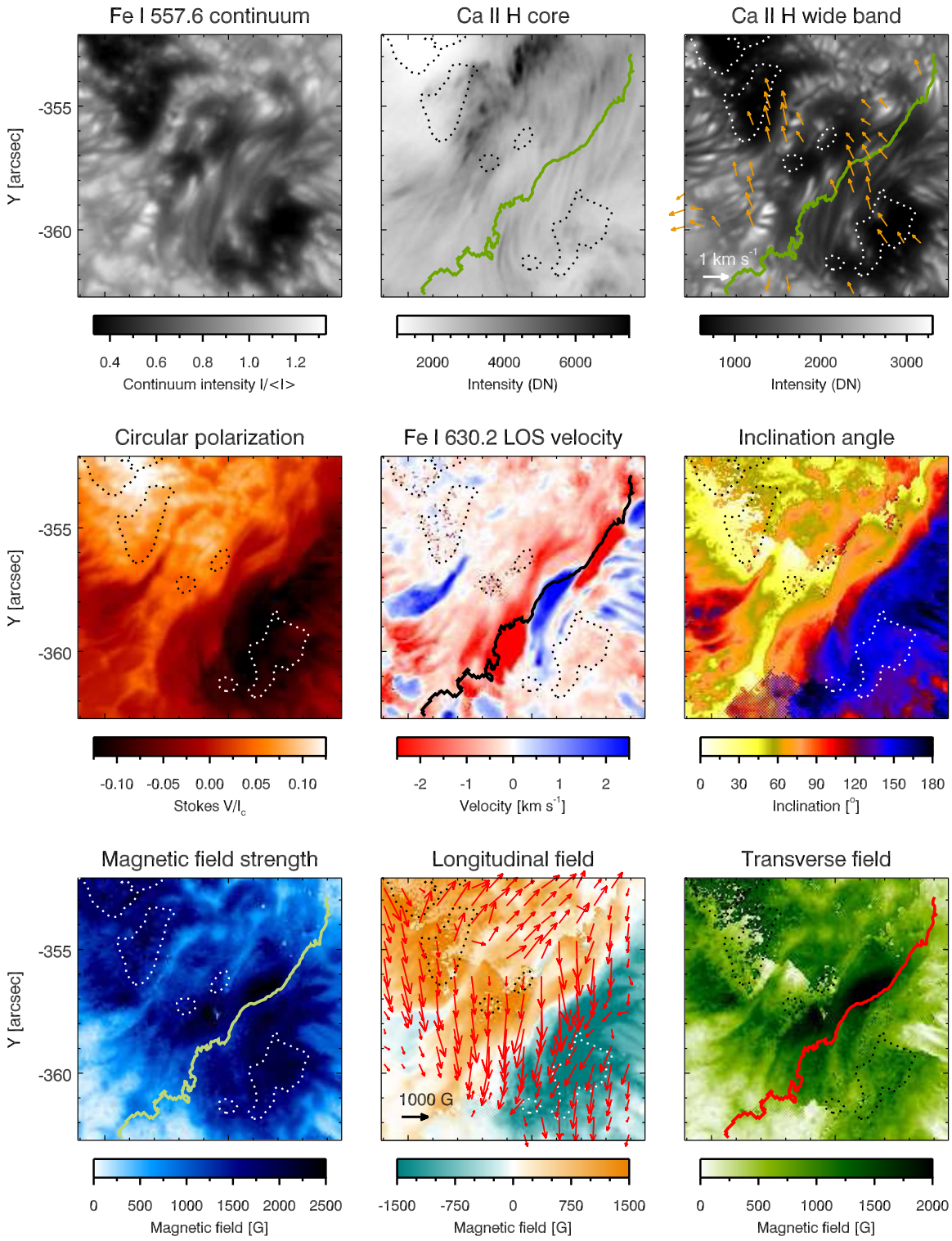

Figure 11. From top to bottom and from left to right: zoomed images of photospheric continuum intensity, chromospheric Ca II H line core intensity (negative image), wide-band Ca II H line intensity with the horizontal velocities overplotted, circular polarization signal, LOS velocity retrieved by SIR, inclination angle of the vector magnetic field, magnetic field strength, longitudinal magnetic field component with the transverse magnetic field overplotted, and the transverse field component. The contours indicate the PIL; the dotted contours show the location of the umbrae. The FoV is that one indicated in Figure 6 (left panel) with the dotted line square. All maps refer to 09:00:05 UT.

or (2) they act on the magnetic flux below the solar surface. In the latter case, when the distance L between the flux tube footpoints becomes smaller than L_c (defined as the critical separation between the anchor points of an emerging flux tube, see, e.g., Priest 1982), the pressure becomes greater than the magnetic tension and the Ω-loop will submerge (see, e.g., Figure 11 in Takizawa et al. 2012). However, in our case this hypothesis can be promptly settled out due to the presence of the upward patch, hardly justifiable in such a scenario.

Therefore, the hypothesis that seems to be the most suitable for the interpretation of the analyzed data, taking into account the location, the values, and the persistency of the detected

velocity fields, is that we are detecting the LOS component of Evershed flows.

In this regard, Lites et al. (2002) suggested that the field lines harboring the Evershed flow bend down through or just beyond the visible outer penumbral boundary. In their analysis, based on the hypothesis that all plasma flows are directed along the magnetic field (parallel or antiparallel), the observed Doppler shifts were interpreted as being due to at least *two systems* of high-velocity steady flows, converging above the PIL and having the same origin as the classical Evershed flow. In the δ spot analyzed by Lites et al. (2002), due to its proximity to the solar limb, the LOS passes through the interleaved magnetic field lines, crossing first the flux tubes where the plasma motion occurs in one direction and then those where the plasma flows in the opposite direction (see, e.g., Figure 11 in Lites et al. 2002). This suggests that the Evershed flows originating from the two opposite polarity umbrae within the δ spot slip past one another in the convergence zone, bend downward, and dive in the sub-photospheric layers.

We can therefore try to verify whether in the δ spot analyzed in this paper, the observed upward and downward motions can be ascribed to the LOS component of Evershed flows occurring along the magnetic field lines crossing the δ spot PIL, as in the scenario proposed by Lites et al. (2002).

In this regard, we note that the map of the horizontal velocity field shown in Figure 8 indicates that in the region close to the δ spot PIL, the majority of arrows are directed from the negative umbra core toward the positive one, indicating that the horizontal flow we observe is mainly directed along this path. If we complement this result with the information that can be inferred from Figure 11, where we show zoomed maps focusing on the δ spot PIL and its surroundings, we can deduce that along and near the δ spot PIL, the magnetic field is quite strong (1200–2200 G) and almost horizontal (80°–90°), especially in coincidence with strong downward and upward patches. Note also that the magnetic field lines along the δ spot PIL exhibit some shearing, which seems to be higher in correspondence with the downflow patches, and lower where the upflow is observed. The inclination angle between the PIL and these transverse magnetic fields is about 45°. Figure 10, which shows a comparison between some magnetic and dynamic properties in sections of an LB of the leading spot and of the δ spot PIL, is quite illustrative in showing that in the latter region the magnetic field is very strong and almost horizontal, with conditions not favorable to convection (like in a LB), but most likely very favorable to the Evershed flow occurrence.

In order to verify this interpretation, we further analyze Figure 11, where we can see that the upflowing patches coincide with regions of lower longitudinal magnetic field strength characterized by an almost horizontal magnetic field configuration. Actually, the upflow patch spatially coincides with the most intense horizontal velocity field in the region, whereas the downward patches do not show any correspondence with the horizontal motions that have been detected with the LCT technique, from the images in the wide band of the Ca II H line. This effect might be an indication of different heights at which we observe the "interleaved magnetic field lines" in fluted penumbral filaments hosting Evershed flows occurring in opposite directions.

5. CONCLUSIONS

We studied the morphology, dynamics, and magnetic field configuration of NOAA AR 11267 hosting a δ spot using *SDO*/HMI observations and a high-resolution data set of spectropolarimetric measurements acquired with the CRISP at the SST. The region between the opposite polarities of the δ spot showed the presence of dark filaments wrapped around the two umbra cores. This region was also characterized by steady upward and downward plasma flows of $\sim$3 km s^{-1}, and shear of the magnetic field.

The above plasma motions derived from both *SDO*/HMI and CRISP measurements are subsonic, contrary to the strong, supersonic downflows detected, e.g., by Martínez Pillet et al. (1994), who also established that they were coincident with a highly sheared magnetic field at the neutral line, as found in our study. Prasad Choudhary & Deng (2012), who also reported supersonic downflows that lasted for about six hr, proposed that a possible origin of these motions could be the bending of penumbral Evershed flow channels as neutral lines are formed in δ spots. Taking into account that a normal spot has Evershed flow channels where the plasma flows almost parallel to the solar surface, these channels can get bent downward when they encounter the strong vertical field of another sunspot. When this interface region is located between two opposite polarities sharing the same penumbra (i.e., the δ spot), the presence of strong downflows indicates the abrupt bending of the penumbral filaments in proximity to the PIL. Denker et al. (2007), from the analysis of subsonic persistent flows measured in a δ spot, established that they should be related to the magnetic field lines harboring the more horizontal Evershed flow channels. They stated that the proximity of two penumbrae with colliding outflows could result either in the subduction of one flow pattern or to horizontal deflection of the opposing flows.

In the δ spot considered in our study, in the *gappy penumbra* facing the two opposite magnetic polarities, the plasma motion (which we observe in the LOS component) takes place in the region hosting curved filaments, which are almost tangential to the opposite polarity umbral cores. This situation gives rise to the complex LOS velocity pattern we observe, where both subsonic downflows and upflows are detected. In the previous section, we investigated three possible scenarios to interpret these motions: emergence of new magnetic flux, submergence of an Ω-loop, and presence of velocity fields related to the Evershed flows. From the analysis of our results we could exclude the first two hypotheses, i.e., emergence or submergence of magnetic flux. On the other hand, if we complement the result of the LOS velocity pattern with that obtained using the LCT technique, showing horizontal motions of the order of $\sim$1 km s^{-1} directed toward the positive umbra core, we can conclude that these motions may be due to the Evershed flow in this region. In particular, the scenario that seems to fit our observations better is the one proposed by Lites et al. (2002), characterized by at least two systems of high-velocity steady flows converging above the PIL.

More precisely, from the location of the upward and downward patches and the area hosting the horizontal motions, we can deduce that along the PIL there are two systems of fluted penumbral filaments, which are highly sheared and facing each other, such that in one of them we observe an Evershed flow directed from the negative to the positive umbra, while the other, characterized by downflows, might be related either to a motion in the opposite direction, occurring at different heights, or to an even more complex configuration that is not possible to disentangle with the current observations.

The analysis of new and even higher-resolution observations than those analyzed in our study, which will be carried out in

the future with larger aperture telescopes such as the GREGOR telescope (Schmidt et al. 2012), the European Solar Telescope (Collados et al. 2010), and the Advanced Technology Solar Telescope (Keil et al. 2010), shall allow us to shed more light on the complex interplay between plasma and magnetic fields in δ spots.

We thank an anonymous referee for useful suggestions that helped us to improve the paper. The authors wish to thank the SST staff for its support during the observing campaigns. The Swedish 1 m Solar Telescope is operated on the island of La Palma by the Institute for Solar Physics of Stockholm University in the Spanish Observatorio del Roque de los Muchachos of the Instituto de Astrofísica de Canarias. The *SDO*/HMI data used in this paper are courtesy of NASA/*SDO* and the HMI science team. Use of NASA's Astrophysical Data System is gratefully acknowledged. S.L.G. thanks D.L. Distefano for his help in editing the *SDO*/HMI movie. The research leading to these results has received funding from the European Commissions Seventh Framework Programme under the grant agreements No. 284461 (eHEROES project), No. 312495 (SOLARNET project), and No. 606862 (F-Chroma project). This work was also supported by the Instituto Nazionale di Astrofisica (PRIN INAF 2010), and by the Università degli Studi di Catania.

REFERENCES

Balthasar, H. 1988, A&AS, 72, 473
Balthasar, H., Beck, C., Louis, R. E., Verma, M., & Denker, C. 2014, A&A, 562, L6
Berger, T. E., & Berdyugina, S. V. 2003, ApJL, 589, L117
Bharti, L., Rimmele, T., Jain, R., Jaafrey, S. N. A., & Smartt, R. N. 2007, MNRAS, 376, 1291
Bruzek, A. 1967, SoPh, 2, 451
Collados, M., Bettonvil, F., Cavaller, L., et al. 2010, AN, 331, 615
de la Cruz Rodríguez, J., Kiselman, D., & Carlsson, M. 2011, A&A, 528, A113
de la Cruz Rodríguez, J., Löfdahl, M., Hillberg, T., et al. 2014, arXiv:1406.0202
de la Cruz Rodríguez, J., Rouppe van der Voort, L., Socas-Navarro, H., & van Noort, M. 2013, A&A, 556, A115
Deng, N., Liu, C., Prasad Choudhary, D., & Wang, H. 2011, ApJL, 733, L14
Denker, C., Deng, N., Tritschler, A., & Yurchyshyn, V. 2007, SoPh, 245, 219
Denker, C., & Wang, 1998, ApJ, 502, 493
Dravins, D., Lindegren, L., & Nordlund, A. 1981, A&A, 96, 345
Evershed, J. 1909, MNRAS, 69, 454
Gingerich, O., Noyes, R. W., Kalkofen, W., & Cuny, Y. 1971, SoPh, 18, 347
Henriques, V. M. J. 2012, A&A, 548, A114
Keil, S. L., Rimmele, T. R., Wagner, J., & ATST Team., 2010, AN, 331, 609
Kunzel, H., Mattig, W., & Schroter, E. H. 1961, Sterne, 9/10, 198
Leka, K. D., Barnes, G., Crouch, A. D., et al. 2009, SoPh, 260, 83
Lites, B. W., Socas-Navarro, H., & Skumanich, A. 2002, ApJ, 575, 1131
Markwardt, C. B. 2009, in ASP Conf. Ser. 411, Astronomical Data Analysis Software and Systems XVIII, ed. D. A. Bohlender, D. Durand, & P. Dowler (San Francisco, CA: ASP), 251
Martínez Pillet, V., Lites, B. W., Skumanich, A., & Degenhardt, D. 1994, ApJL, 425, L113
Min, S., & Chae, J. 2009, SoPh, 258, 203
November, L. J., & Simon, G. W. 1988, ApJ, 333, 427
Pesnell, W. D., Thompson, B. J., & Chamberlin, P. C. 2012, SoPh, 275, 3
Prasad Choudhary, D., & Deng, N. 2012, ASP Conf. Ser. 43, Magnetic Fields from the Photosphere to the Corona, ed. T. R. Rimmele & V. M. Collados (San Francisco, CA: ASP)
Priest, E. R. 1982, in Solar Magnetohydrodynamics (Dordrecht: Reidel), 291
Romano, P., Frasca, D., Guglielmino, S. L., et al. 2013, ApJL, 771, L3
Ruiz Cobo, B., & del Toro Iniesta, J. C. 1992, ApJ, 398, 375
Scharmer, G. B., Bjelksjo, K., Korhonen, T. K., Lindberg, B., & Petterson, B. 2003a, Proc. SPIE, 4853, 341
Scharmer, G. B., Dettori, P. M., Lofdahl, M. G., & Shand, M. 2003b, Proc. SPIE, 4853, 370
Scharmer, G. B., Narayan, G., Hillberg, T., et al. 2008, ApJL, 689, L69
Scherrer, P. H., Schou, J., Bush, R. I., et al. 2012, SoPh, 275, 207
Schlichenmaier, R., Rezaei, R., Bello González, N., & Waldmann, T. A. 2010, A&A, 512, L1
Schmidt, W., von der Lühe, O., Volkmer, R., et al. 2012, AN, 333, 796
Schnerr, R. S., de La Cruz Rodríguez, J., & van Noort, M. 2011, A&A, 534, A45
Shimizu, T., Katsukawa, Y., Kubo, M., et al. 2009, ApJL, 696, L66
Shine, R. A., Title, A. M., Tarbell, T. D., et al. 1994, ApJ, 430, 413
Spadaro, D., Billotta, S., Contarino, L., Romano, P., & Zuccarello, F. 2004, A&A, 425, 309
Takizawa, K., Kitai, R., & Zhang, Y. 2012, SoPh, 281, 599
Tang, F. 1983, SoPh, 89, 43
Thomas, J. H., & Weiss, N. O. 2004, ARA&A, 42, 517
van Noort, M., Rouppe van der Voort, L., & Lofdahl, M. G. 2005, SoPh, 228, 191
Verma, M., & Denker, C. 2011, A&A, 529, A153
von der Lühe, O. 1998, NewAR, 42, 493
Zirin, H., & Liggett, M. A. 1987, SoPh, 113, 267
Zuccarello, F., Battiato, V., Contarino, L., et al. 2005, A&A, 442, 661